J. Chem. Thermodynamics 158 (2021) 106466

Contents lists available at ScienceDirect

J. Chem. Thermodynamics

journal homepage: www.elsevier.com/locate/jct

Phase diagrams of aqueous solutions of the potassium salts of malonic, succinic, and glutaric acids

Julia L. Roskam [1], Kristen L. Nowak, Karl T. Taylor, Samuel R. Rendler [2], Keith D. Beyer *

Department of Chemistry & Biochemistry, University of Wisconsin-La Crosse, 1725 State St., La Crosse, WI 54601, USA

ARTICLE INFO

Article history:
Received 17 August 2020
Received in revised form 19 March 2021
Accepted 20 March 2021
Available online 24 March 2021

Keywords:
Malonic acid
Potassium hydrogen malonate
Succinic acid
Potassium hydrogen succinate
Glutaric acid
Potassium hydrogen glutarate
Phase diagram
Solubility

ABSTRACT

Phase equilibria in aqueous systems of 1:1 and 2:1 KOH and the following dicarboxylic acids have been studied: malonic, succinic, and glutaric. The temperature of thermal transitions was determined in solutions of known composition using Differential Scanning Calorimetry. The identity of the least soluble solid was determined by a combination of X-ray crystallography and infrared spectroscopy. Combining these data facilitated construction of a partial phase diagram for each system. In general, the potassium salts of carboxylic acids studied here are at least as soluble as their sodium salt analogs, and generally more soluble than the parent acids with some temperature dependent exceptions. While the single potassium salts readily formed in the respective systems studied here, we did not observe the formation of any of the double salts.

1. Introduction

The phase equilibria of aqueous dicarboxylic acid salts have been little studied and their solubilities are missing from standard compilations [1–3], and online databases [4]. However, knowledge of their physical chemical properties has received renewed interest as their constituent species are found in environmental systems. Field measurements have shown that the major chemical components of aerosols in the free and upper troposphere (UT) include organic and inorganic compounds and mineral dust [5,6]. With respect to the organic fraction, dicarboxylic acids (DCA) have been found in a range of environments, particularly for aerosols that have undergone chemical aging [7]. Organics, potassium ions, and potassium salts have been shown to be present in large numbers of aerosols in field studies due to biomass burning [8-10]. Field and lab studies have shown that metal ions can combine with the conjugate bases of dicarboxylic acids to form carboxylate salts that can crystallize in atmospheric aerosols in dry atmospheric and/or low temperature conditions [11,14]. For example:

$$nK^{+}(aq) + H_{(2-n)}C_4H_4O_4^{-n}(aq) \rightarrow K_nH_{(2-n)}C_4H_4O_4(s) \quad (1)$$

where n equals one or two. According to recent studies the organic and potassium ions will remain in solution since their possible compounds have low vapor pressures [12,13]. Thus, potassium oxalate salts could crystalize in solution when the aqueous particles experience either cold or dry conditions in the atmosphere [14]. We previously studied the solubilities of the sodium salts of dicarboxylic acids [15,16] and this work is a continuation of that work with metal organic salts.

2. Experimental

2.1. Sample preparation

Solutions studied in our experiments were made by mixing chemicals as listed in Table 1 with deionized water. Typically, solutions of increasing composition solute were made in roughly 0.05 mass fraction (w) increments until solids would no longer dissolve after 24 h of stirring and heating to 323 K. Samples were maintained in glass stoppered containers to avoid water evaporation. The average ratio of KOH to dicarboxylic acid in the systems studied are as follows: $KHC_3H_2O_4$ (1.002 ± 0.002), $K_2C_3H_2O_4$ (2.003 ± 0.004), $KHC_4H_4O_4$ (1.002 ± 0.006), $K_2C_4H_4O_4$ (2.004 ± 0.005), $KHC_5H_6O_4$ (1.000 ± 0.001), $K_2C_5H_6O_4$ (1.9999 ± 0.0004). Throughout this

* Corresponding author.
E-mail address: kbeyer@uwlax.edu (K.D. Beyer).
[1] Present address: Department of Neuroimmunology, Mayo Clinic, Rochester, MN, USA.
[2] Present address: Millipore Sigma, Sheboygan Falls, WI, USA.

https://doi.org/10.1016/j.jct.2021.106466
0021-9614/

Table 1
Chemical samples used in this study.

Chemical name	Chemical formula	CAS registry	Source	Mass fraction purity	Purification method
Malonic Acid	$C_4H_6O_4$	141–82-2	Acros	>0.99[a]	None
Succinic Acid	$C_4H_6O_4$	110–15-6	Sigma-Aldrich	>0.99[a]	None
Glutaric Acid	$C_5H_8O_4$	110–94-1	Acros Organics	>0.99[a]	None
Potassium Hydroxide	KOH	1310–58-3	Fisher Scientific	0.995 ± 0.008[b]	None
Potassium Hydrogen Malonate	$KHC_3H_2O_4$	926–71-6	*in situ*[c]	[d]	None
Potassium Hydrogen Succinate	$KHC_4H_4O_4$	34717–22-1	*in situ*[c]	[d]	None
Potassium Trihydrogen Disuccinate	$KH_3(C_4H_4O_4)_2$	51658–28-7	*in situ*[c]	[d]	None
Potassium Hydrogen Glutarate	$KHC_5H_6O_4$	37013–85-7	*in situ*[c]	[d]	None
Water	H_2O	7732–18-5	Municipal	≥0.999995	R.O. + D.I.[e]

[a] As reported by the supplier.
[b] As determined by titration of KOH samples with potassium hydrogen phthalate.
[c] These compounds were synthesized from mixtures of commercial compounds in deionized water as described in the text.
[d] Our analysis could not determine the purity of the crystals formed in solution.
[e] Water from the municipal source was purified with a Culligan B-Series Reverse Osmosis (R.O.) system and polished with two Culligan mixed-bed deionizers (D.I.) Purity is as reported by Culligan using conductivity measurements (0.055 μS/cm).

paper values reported as a ± b are mean values (a) with calculated standard deviation (b) = $\sqrt{\frac{\sum(x-\bar{x})^2}{(n-1)}}$, where x is an individual datum, $\bar{x}$ is the mean value, and n is the number of samples.

2.2. Species identification

Infrared spectroscopy was used to identify when ice formed and melted in our samples. The identity of the salt that precipitates from our sample solutions was confirmed by a combination of X-ray crystallography (unit cell determination) and infrared spectroscopy. The unit cell determination was performed at the Molecular Structure Laboratory in the Chemistry Department at the University of Wisconsin-Madison. Details of how these experiments are performed can be found in the Supporting Information of Kissinger *et al.* [15], which is available free of charge via the Internet at http://pubs.acs.org. Briefly, a representative single crystal is removed from a saturated solution at room temperature and placed in the instrument for unit cell determination, also at room temperature. The identity of the solid is based on a match of the unit cell parameters reported to the Cambridge Crystallographic Database (CSD) or the Inorganic Crystal Structure Database (ICSD). (X-ray crystallography was utilized for all systems studied in this paper except the $K_2C_5H_6O_4/H_2O$ system, which is discussed in the Results section.) Once the identity of a solid was determined for one composition, we concluded the pattern of absorption bands in the corresponding infrared spectra constituted the infrared "fingerprint" of that compound, which is shown for each system where salts formed in the Results section. The presence of the unique set of bands in other samples confirmed the presence of the same solid. In addition, consistency (non-discontinuity) in the *liquidus* temperatures in the composition series was additional evidence for the presence of the same solid as that identified in X-ray crystallography and/or infrared spectroscopy experiments.

Infrared spectra were acquired using a temperature controlled, air sealed cell, which is described elsewhere [16]. Temperature control of the sample was achieved by resistive heating with the cooling source being liquid nitrogen in contact with the cell. Two μL of the liquid sample was placed on a ZnSe window and compressed with a second ZnSe window placed in the beam path of a Bruker Tensor 37 FTIR with a DTGS detector at 4 cm^{-1} resolution. Temperature calibration of the cell was achieved by observing the melting phase transition of several substances: HPLC grade water, decane, octane and acetic anhydride all supplied by Aldrich, and covering the range 273–200 K [17].

2.3. Differential scanning calorimetry

Thermal data were obtained with a Mettler Toledo DSC1 instrument. The instrument was purged with high purity nitrogen gas. Our accuracy is estimated to be ± 0.9 K with a probability of 0.94 based on a four point temperature calibration using indium, HPLC grade water, anhydrous, high purity (99%+) octane, and anhydrous, high purity heptane (99%+) from Aldrich, the latter three stored under nitrogen. The details of standard temperature calibration and instrument reproducibility can be found in Schubnell [18]. The average value of the melting point and standard deviation of HPLC grade water in seven experiments after DSC calibration is 273.3 ± 0.2 K.

Samples sizes were typically (20 ± 5) mg using 40 μL aluminum pans with sealed lids. A typical experiment consisted of initially cooling the sample from 298 K to 183 K at 10 K per minute. The sample was then held at 183 K for five minutes, and then temperature increased 1 K per minute to 298 K or a temperature that was expected to be at least five degrees above the last phase transition.

3. Results and discussion

3.1. $KHC_3H_2O_4/H_2O$

For this system we made samples that covered a range of compositions 0.10 to 0.65 w $KHC_3H_2O_4$. Raw DSC data are provided in Table 2. In our DSC experiments, we observed some general trends when cooling and heating the samples. All samples had a glass transition (measured in the warming segment) with an average value for the onset temperature of (224.8 ± 0.8) K. This indicates the samples did not completely crystallize when cooled to 183 K. This observation is further confirmed by crystallization events in the warming segment subsequent to the glass transition. Several endothermic and exothermic events were observed in many samples, indicating solids formed, thermally decomposed, followed by recrystallization of the melt. A typical thermogram for a solution in this system is given in Fig. S1 (w = 0.5998 $KHC_3H_2O_4$). This sample undergoes the series of thermal transitions we described (see figure caption for detail). However, we note that the relative size of the melt/recrystallization transitions (which is proportional to mass of sample undergoing transition) is very small compared to the large transitions for ice melting and salt dissolution. Thus, the fraction of the sample undergoing these transitions is very minor. The identity of the species undergoing the major transitions is confirmed by the IR spectra of a sample of the same composition

Table 2
Phase transitions in the system $KHC_3H_2O_4/H_2O$ as determined by DSC experiments. Composition is given in mass fraction (w), T_g is the onset glass transition temperature, T_e is the eutectic temperature, and T_l is the *liquidus* temperature of the indicated phase, at pressure 99.2 kPa.[a]

w $KHC_3H_2O_4$[b]	T_g/K[c]	T_e/K[c]	T_l/K[c]	Phase field[d]
0.1000	224.3	264.3	271.8	Ice
0.2000	224.6	264.3	269.2	Ice
0.2999	224.3	264.3	267.4	Ice
0.3498	224.4	264.2	265.8	Ice
0.4000	224.7	264.2	267.4	$KHC_3H_2O_4$
0.4500	224.8	264.2	271.0	$KHC_3H_2O_4$
0.4998	224.4	264.1	273.0	$KHC_3H_2O_4$
0.5502	224.4	264.0	276.4	$KHC_3H_2O_4$
0.5998	226.9	264.0	279.5	$KHC_3H_2O_4$
0.6499	225.0	264.1	281.6	$KHC_3H_2O_4$

[a] Experimental pressure was not controlled beyond the typical range of atmospheric pressure, (99.2 ± 2.9) kPa (station pressure).
[b] Mass fraction uncertainty, U = 0.001 (0.95 confidence level).
[c] Temperature uncertainty, U = 0.9 K (0.94 confidence level).
[d] Melting of ice was identified by infrared (IR) spectroscopy of thin films as described in the Experimental Section. Identity of salt phase field is given by a combination of X-ray crystallography and IR analysis.

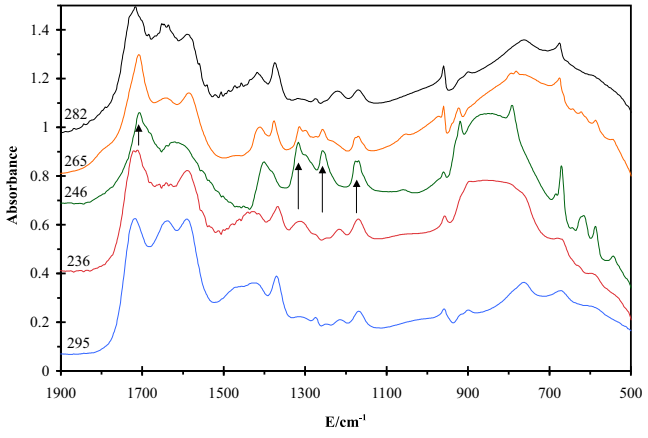

Fig. 1. Temperature series of infrared spectra for a w = 0.5998 $KHC_3H_2O_4$ sample (same composition as for the thermogram shown in Fig. S1), where E represents energy in units of wavenumbers (cm^{-1}). Temperature of each spectrum is given in the figure in Kelvin. For clarity, spectra are offset as follows: 295 K (0); 236 K (+0.3); 246 K (+0.5); 265 K (+0.7); 282 K (+0.9). Cooling series: sample is initially all liquid at 295 K, as the sample is cooled ice crystallizes at 236 K as indicated by the appearance of the large, broad band centered at 855 cm^{-1}. Minimum temperature reached was 218 K. The sample was then warmed with crystallization of $KHC_3H_2O_4$ at 246 K as indicated by the changes in the bands marked by arrows (see Section 3.1 for details). Ice melted at the eutectic at 265 K as the broad band at 855 cm^{-1} disappears. $KHC_3H_2O_4$ continually dissolved upon further warming until characteristic absorption bands for the salt had disappeared by 282 K.

as shown in Fig. 1. We have noted the most significant shifts due to crystallization of $KHC_3H_2O_4$ with arrows in the figure. In all cases, appearance of these band shifts indicated formation of solid $KHC_3H_2O_4$, and their disappearance indicated dissolution of the solid. On the high energy side, we observed a band at 1719 cm^{-1} shifts to 1708 cm^{-1} and broadens slightly. At 1313 cm^{-1} we observed a small, broad band that shifts to 1317 cm^{-1} while increasing in intensity and sharpens. Third is a very small band at 1249 cm^{-1} that increases to a medium band intensity and sharpens to 1257 cm^{-1}. Last is a medium, sharp band at 1169 cm^{-1} that bifurcates with maximum absorbances at (1176 and 1168) cm^{-1}. We observed other, smaller shifts as well, but these changes in the IR spectrum were the easiest to see. Thus, it was clear when eutectic and final melt (ice) or dissolution (salt) were observed in the IR spectra, which were then correlated with the transitions observed in the thermograms. This facilitated the construction of a phase diagram as given in Fig. 2. Additional evidence for the formation of $KHC_3H_2O_4$ from our solutions was X-ray crystallographic unit cell determinations; a single crystal that precipitated from a 0.5640 w $KHC_3H_2O_4$ solution was analyzed with this method (we did not perform a DSC experiment on this sample). The solid was determined to be $KHC_3H_2O_4$ by a match of the crystallographic unit cell parameters [19] in the Cambridge Crystallographic Database (CSD), which are tabulated in Table S1.

The average eutectic value from the thermograms is (264.1 ± 0.2) K. We determined the eutectic composition to be 0.3671 w $KHC_3H_2O_4$ by a fit to our ice melting points and the solubility values for the salt following the equation:

$$T = A_2w^2 + A_1w + A_0 \quad (2)$$

where w is the mass fraction of salt in the aqueous solution, T is temperature in Kelvin, and the values of A_2, A_1, and A_0 are given in Table 3 for each equation. The two equations were solved simultaneously to yield the eutectic composition. With this composition determined, we then calculated the predicted eutectic temperature from the fit equations to be 265.4 K. This value is 1.3 K higher than our average eutectic value from the thermogram data. This results from the observation that the onset of the eutectic transition was immediately followed by a partial, small recrystallization event in all of our samples, thus making an onset temperature difficult to determine from the thermograms (see example thermogram in Fig. S1). Therefore, we recommend the value calculated from the intersection of the *liquidus* curves as closer to the correct eutectic temperature.

We previously studied the $NaHC_3H_2O_4/H_2O$ [15] and $H_2C_3H_2O_4/H_2O$ [20] systems and determined that the least soluble solids were $NaHC_3H_2O_4{\cdot}H_2O$ and $H_2C_3H_2O_4$, respectively. The solubility data are shown as diamonds for $NaHC_3H_2O_4{\cdot}H_2O$ and as a dotted line for $H_2C_3H_2O_4$ in Fig. 2 for comparison to the $KHC_3H_2O_4$ data. It is readily seen $KHC_3H_2O_4$ is much more soluble than $NaHC_3H_2O_4{\cdot}H_2O$. However, there is a crossing point for the solubility of $KHC_3H_2O_4$ and $H_2C_3H_2O_4$ at 275 K. Therefore, at T > 275 K malonic acid is the least soluble compound, whereas at lower temperatures, $KHC_3H_2O_4$ is less soluble. Thus, in solutions (such as atmospheric aerosols) where both Na^+ and K^+ may be present with hydrogen malonate

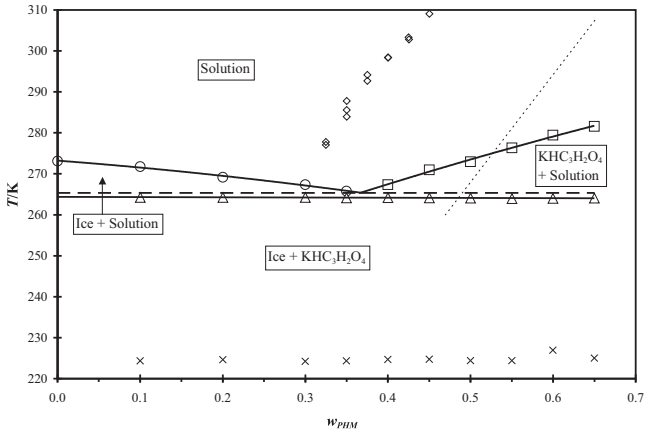

Fig. 2. Partial solid/liquid phase diagram of the $KHC_3H_2O_4/H_2O$ system constructed from our DSC data. Solid lines are phase boundaries, horizontal dashed line is the eutectic line calculated from the intersection of the two *liquidus* lines, and w_{PHM} is the mass fraction $KHC_3H_2O_4$. Symbols are: ○ ice melt, □ $KHC_3H_2O_4$ dissolution, △ eutectic transition, x glass transition. Shown for comparison are the solubility of $NaHC_3H_2O_4$ from Kissinger, *et al.* [15] (◇), and fit of the aqueous solubility of $H_2C_3H_2O_4$ [20] (dotted line).

Table 3
Fit parameters for solid/liquid equilibria.

Region	A_2	A_1	A_0
$KHC_3H_2O_4/H_2O$			
Ice	−16.28	−15.36	273.2
$KHC_3H_2O_4$	−21.03	79.23	239.1
$K_2C_3H_2O_4/H_2O$			
Ice	−176.8	24.22	272.1
$KHC_4H_4O_4/H_2O$			
Ice	−298.4	6.165	273.2
$KH_3(C_4H_4O_4)_2$	−273.6	320.9	227.4
$K_2C_4H_4O_4/H_2O$			
Ice	−56.93	−22.64	273.3
$KHC_4H_4O_4$	−492.7	525.2	167.2
$KHC_5H_6O_4/H_2O$			
Ice		−21.51	273.2
$KHC_5H_6O_4$		253.3	190.1
$K_2C_5H_6O_4/H_2O$			
Ice	−28.36	26.98	273.2

ions, we would expect $NaHC_3H_2O_4 \bullet H_2O$ to precipitate before $KHC_3H_2O_4$. However, at low pH either $KHC_3H_2O_4$ or malonic acid will be the least soluble solid depending on temperature.

3.2. $K_2C_3H_2O_4/H_2O$

This system was a challenge to study. We made solutions with predicted $K_2C_3H_2O_4$ composition in the range 0.097–0.7 *w* $K_2C_3H_2O_4$. We did not observe any evidence for salt formation in either DSC or IR experiments. Thus, we refer to the composition of samples in this system as the "equivalent" mass fraction $K_2C_3H_2O_4$ (w_{eq}). We did observe that potassium hydroxide (KOH) and $H_2C_3H_2O_4$ readily dissolved in water at lower compositions ($w_{eq} < 0.5$), but at higher mass fractions solutions had to be heated to ensure dissolution. For the lower mass fractions ($w_{eq} \leq 0.6$), we observed ice formation and a glass transition, but again, no evidence for salt formation. Raw DSC data for glass transition and ice melting temperatures are provided in Table 4. We also studied larger sample masses in DSC experiments (to increase nucleation probabilities) up to 133 mg, but we observed no salt formation in these larger samples. For a solution at 0.6993 w_{eq} $K_2C_3H_2O_4$ we did not observe either ice or salt formation in our DSC or IR experiments. Thus, there appears to be either a significant hindrance to salt formation in this system, or the solubility of $K_2C_3H_2O_4$ is extremely high. Colleagues at the Molecular Structure Laboratory at the University of Wisconsin-Madison performed exhaustive searches of the CSD, ICSD, and crystallography literature, and found no record of structures for $K_2C_3H_2O_4$ [21]. In two of the higher mass fraction samples (0.5981 w_{eq} and 0.6998 w_{eq}) we observed crystal formation after storing the approximately 5 mL solution at room temperature for several weeks. A single crystal from each of these samples was used for unit cell determination by single crystal X-ray crystallography. The solid was determined to be $KHC_3H_2O_4$ by a match of the unit cell data [19] in the CSD for both samples, which are given in Table S1. This is an unexpected result, and points to the difficulty in forming the expected $K_2C_3H_2O_4$ crystal in a solution that is 2:1 in K^+:$C_3H_2O_4^{2-}$ on a mole basis. We considered the possibility that $HC_3H_2O_4^-$ may be a significant fraction of the ion composition in solution due its equilibria with the malonate ion in water. The pK_a of $HC_3H_2O_4^-$ is 5.69 resulting in a pK_b value for malonate ion of 8.31 [17]. Given the initial malonate ion concentrations in our solutions due to its stoichiometric neutralization with KOH, the malonate ion would be only 0.003–0.009% reacted to $HC_3H_2O_4^-$. Thus, presence of significant $HC_3H_2O_4^-$ is unlikely to be the explanation for $KHC_3H_2O_4$ crystals in our samples.

Table 4
Glass and ice melting transitions in the system 2:1 KOH:$H_2C_3H_2O_4$ in H_2O as determined by DSC experiments. For simplicity, composition is given in equivalent mass fraction $K_2C_3H_2O_4$ (w_{eq}), T_g is the onset glass transition temperature, and T_i is the *liquidus* temperature for ice, at pressure 99.2 kPa.[a]

w_{eq} $K_2C_3H_2O_4$[b]	T_g/K[c]	T_i/K[c,d]
0.097		272.2
0.1883	193.8	268.7
0.2001	194.6	268.5
0.2998	192.6	262.9
0.3003	193.8	262.0
0.4003	193.3	253.5
0.5003	192.6	240.9
0.5003	195.1	242.6
0.5006	193.7	241.8
0.5981		223.1

[a] Experimental pressure was not controlled beyond the typical range of atmospheric pressure, (99.2 ± 2.9) kPa (station pressure).
[b] Mass fraction uncertainty, $U = 0.001$ (0.95 confidence level).
[c] Temperature uncertainty, $U = 2$ K (0.94 confidence level).
[d] Melting of ice was identified by infrared spectroscopy of thin films as described in the Experimental section of the paper.

In some samples where ice was observed (0.1883–0.5006 w_{eq} $K_2C_3H_2O_4$), we also observed a glass transition. The average onset of the glass transition on warming was (193.7 ± 0.9) K. A typical DSC thermogram for this system (0.3003 w_{eq} $K_2C_3H_2O_4$) is shown in Fig. S2. Raw data for this system is provided in Table 4 and plotted in Fig. 3 in units of equivalent mass fraction $K_2C_3H_2O_4$ (since the compound did not form in our solution) along with solubilities for $Na_2C_3H_2O_4 \cdot H_2O$ [15] and $H_2C_3H_2O_4$ [20] for comparison purposes. We fit the ice melting data to Eq. (1), and the parameters are listed in Table 3. We note that the disodium monohydrate salt of malonic acid is less soluble than malonic acid itself, similar to the case for the monosodium salt. We also note that the crystal structure of the disodium salt of malonic acid had not been known previously to our study [15]. Thus, it may not be surprising that the dipotassium salt structure has not been reported. Given that the monopotassium salt of malonic acid is much more water soluble than the monosodium salt, it seems reasonable to predict the same for the dipotassium salt as compared to the disodium salt. Also, we feel the fact that we formed $KHC_3H_2O_4$ from two high composition solutions that were 2:1 in K^+:$C_3H_2O_4^{2-}$ indicates the likely large barrier to nucleation of $K_2C_3H_2O_4$ in aqueous solution. Thus, in an

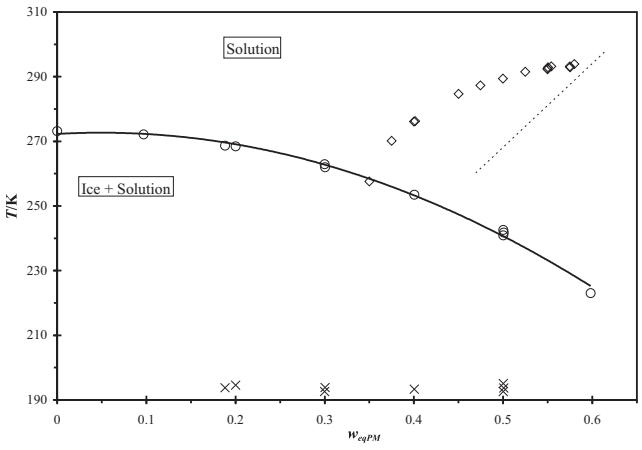

Fig. 3. Ice/solution phase equilibria in aqueous solutions containing a 2:1 ratio of KOH:$H_2C_3H_2O_4$ constructed from our DSC data. Solid curve is the ice/liquid phase boundary, and w_{eqPM} is the equivalent mass fraction $K_2C_3H_2O_4$. Symbols are: ○ ice melting, × glass transition. Shown for comparison are the solubility of $Na_2C_3H_2O_4 \cdot H_2O$ from Kissinger, *et al.* [15] (◇), and fit of the aqueous solubility of $H_2C_3H_2O_4$ [20] (dotted line).

environment where Na^+ and K^+ are present with malonate ions at pH above 7 (sea spray aerosols), the sodium salt would be much more likely to form under dry conditions than the potassium salt.

3.3. $KHC_4H_4O_4/H_2O$

We studied solutions with predicted composition ranging from 0.057 to 0.53 *w* $KHC_4H_4O_4$ for this system. In our DSC experiments, we observed crystallization occurred in both the cooling and warming segments for all samples. This was followed by a general pattern of eutectic and *liquidus* transitions in the warming segment. A typical thermogram for a solution in this system is given in Fig. S3 (predicted 0.3846 *w* $KHC_4H_4O_4$). In order to identify the solid being formed we utilized X-ray crystallography. Crystals made from a predicted 0.4938 *w* $KHC_4H_4O_4$ solution were utilized, and two distinctly different crystal morphologies were present in the sample; therefore, a crystal of each type was used for unit cell determination. One crystal was determined to be polymeric with the unit formula $KH_3(C_4H_4O_4)_2$ named potassium trihydrogen disuccinate by a match to the CSD [22]. The second crystal was determined to be $KHC_4H_4O_4$ by a match to the CSD [23]. Unit cell parameters for our crystals and those from the literature references are given in Table S1. It is unclear whether these two crystal forms are polymorphs with an interconversion temperature, or whether they coexist in a natural state. Given that the crystals were in coexistence in the mother solution in our sample for several weeks before being removed for analysis, it seems the latter state is possible, or at least one compound is in a long-term metastable state. We observed differences in several properties between this system and 2:1 $KOH:H_2C_4H_4O_4$ where evidence points to $KHC_4H_4O_4$ formation in that system as detailed in the next section. Those differences were: solubility, eutectic temperature and composition in aqueous solution, and IR spectra of crystallized samples. Details of these differences are given in Section 3.4. Based on these we propose $KH_3(C_4H_4O_4)_2$ as the major crystal forming in our solutions or possibly a solid solution of $KH_3(C_4H_4O_4)_2$ and $KHC_4H_4O_4$ in solutions of 1:1 $KOH:H_2C_4H_4O_4$. However, the latter would need extensive further investigation to confirm. Therefore, data for this system will be presented as "equivalent" mass fraction $KHC_4H_4O_4$ and utilize the symbol w_{eqPHS} and the compound formed will be presented as $KH_3(C_4H_4O_4)_2$.

Table 5
Phase transitions in the system 1:1 $KOH:H_2C_4H_4O_4/H_2O$ as determined by DSC experiments. Composition is given in equivalent mass fraction $KHC_4H_4O_4$ (w_{eqPHS}), T_g is the onset glass transition temperature, T_e is the eutectic temperature, and T_l is the *liquidus* temperature of the indicated phase, at pressure 99.2 kPa.[a]

w_{eqPHS}[b]	T_g/K[c]	T_e/K[c]	T_l/K[c]	Phase field[d]
0.0571		267.0	272.7	Ice
0.1138	216.4	268.0	271.2	Ice
0.1566	217.9	267.1	270.3	$KH_3(C_4H_4O_4)_2$
0.2028	216.8	268.0	279.6	$KH_3(C_4H_4O_4)_2$
0.2499	217.0	268.0	289.0	$KH_3(C_4H_4O_4)_2$
0.2767		267.4	292.1	$KH_3(C_4H_4O_4)_2$
0.3012	215.2	268.0	296.5	$KH_3(C_4H_4O_4)_2$
0.3846	205.6	267.4	307.1	$KH_3(C_4H_4O_4)_2$
0.4938		267.4	317.0	$KH_3(C_4H_4O_4)_2$
0.5300		265.9	319.8	$KH_3(C_4H_4O_4)_2$

[a] Experimental pressure was not controlled beyond the typical range of atmospheric pressure, (99.2 ± 2.9) kPa (station pressure).
[b] Mass fraction uncertainty, $U = 0.001$ (0.95 confidence level).
[c] Temperature uncertainty, $U = 0.9$ K (0.94 confidence level).
[d] Melting of ice was identified by infrared (IR) spectroscopy of thin films as described in the Experimental Section. Identity of salt phase field is given by a combination of X-ray crystallography and IR analysis, though X-ray data indicate $KHC_4H_4O_4$ may also be present.

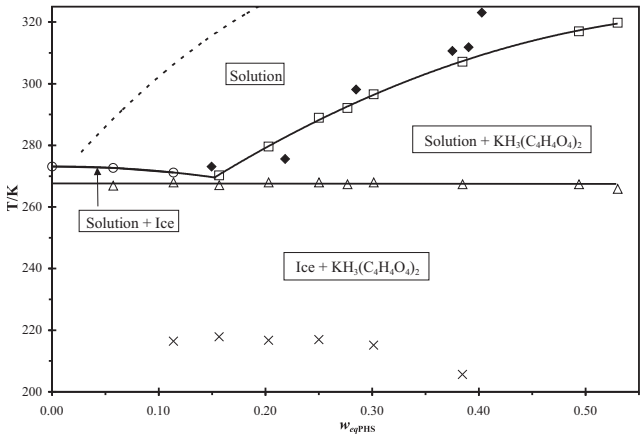

Fig. 4. Phase equilibria in aqueous solutions of 1:1 ratio of $KOH:H_2C_4H_4O_4$ constructed from our DSC data; w_{eqPHS} is the equivalent mass fraction of $KHC_4H_4O_4$. Symbols are: ○ ice melting, □ salt *liquidus*, △ eutectic transition, x onset glass transition temperature. For comparison, ◆ are solubility data from the $NaHC_4H_4O_4/H_2O$ system from Linke [1] plotted as mass fraction $NaHC_4H_4O_4$ (see text). Dotted line is a fit to the solubility of succinic acid also from Linke, and plotted as mass fraction of $H_2C_4H_4O_4$.

Raw DSC data are provided in Table 5, and the transitions for this system observed in DSC experiments are plotted in Fig. 4. The *liquidus* data for each primary phase region were fit to Eq. (1) with the polynomial coefficients given in Table 3. The two equations were simultaneously solved to determine the eutectic composition, 0.1437 w_{eqPHS} and temperature of 267.9 K. The experimental eutectic temperature was determined to be 267.4 ± 0.6 K based on the average onset temperature of the eutectic transition from DSC data. We have labeled the phase region on the phase diagram in Fig. 4 accordingly with the caveat that more information is needed regarding the thermal stability of the two compounds that may form in this system.

The solubility of $NaHC_4H_4O_4$ and succinic acid in water are available in standard compilations [1], and we have plotted these data on our phase diagram in Fig. 4 for comparison purposes. In the $NaHC_4H_4O_4/H_2O$ system $NaHC_4H_4O_4{\cdot}3H_2O$ forms from solutions with $w \leq 0.39$, and $NaHC_4H_4O_4$ forms from solutions with $w \geq 0.39$. It is seen in Fig. 4 the solubility of $NaHC_4H_4O_4{\cdot}3H_2O$ is strikingly similar to that of $KHC_4H_4O_4$, while both are much more soluble than succinic acid. Thus, it is possible in aqueous systems with $HC_4H_4O_4^-$, K^+, and Na^+ present, both salts may precipitate; whereas at low pH where succinic acid is present, it is by far the least soluble salt. Clearly the presence of metals significantly increases the solubility of succinates in water as compared to succinic acid.

We then utilized infrared spectroscopy to identify spectral features in our samples due to salt formation. These experiments also allow us to identify the formation and melting of ice. A series of IR spectra taken at different temperatures is shown in Fig. 5 for the same sample used for crystallographic analysis (0.4494 w_{eqPHS}.) Several spectral features appear to be characteristic of the salt and are indicated by arrows in the figure for a completely frozen sample: an absorption band centered at 1652 cm^{-1} in solution bifurcates to (1673 and 1636) cm^{-1}; a small shoulder at 1343 cm^{-1} changes to a small, broad band; a very small band at 1295 cm^{-1} increases to a broad, medium band; and a very small band at 877 cm^{-1} on top of the broad OH absorption band of water shifts to 893 cm^{-1} and greatly increases in intensity. Other shifts in the spectra were smaller or had significant overlap with water bands. The spectral features we noted were used as the signature for salt formation in our other solutions. We found these features

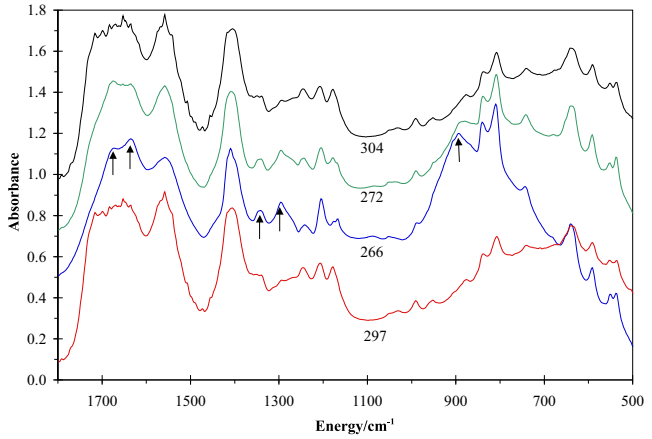

Figure 5. Temperature series of infrared spectra for a 0.4938 w_{eqPHS} sample. Temperature of each spectrum is given in the figure in Kelvin. For clarity, spectra are offset by the following: 297 K (-0.2); 266 K (+0.1); 272 K (+0.4); 304 K (+0.7). Sample is initially all liquid at 297 K. Upon cooling it completely crystalized at 241 K after which warming was commenced. The bands we identified as characteristic of the salt (assumed to be $KH_3(C_4H_4O_4)_2$ – see Section 3.3 and 3.4) are indicated by arrows in the 266 K spectrum, which is just before the eutectic melt (see Section 3.3 for details). Ice melted at the eutectic (the broad band at 855 cm^{-1} disappears) as seen in the 272 K spectrum which is just above the eutectic temperature of 267 K. $KH_3(C_4H_4O_4)_2$ continually dissolved upon further warming until characteristic absorption bands for the salt gradually shift to those observed in solution (304 K). It is difficult to determine the *liquidus* point for the salt in IR experiments as spectral changes become very subtle.

Table 6
Phase transitions in the system 2:1 KOH:$H_2C_4H_4O_4$/H_2O as determined by DSC experiments. Composition is given in equivalent mass fraction $K_2C_4H_4O_4$ (w_{eqPS}) since this salt was not observed to form but rather $KHC_4H_4O_4$, T_g is the onset glass transition temperature, T_{et} is the DSC software calculated onset temperature of the first endothermic transition, and T_l is the *liquidus* temperature of the indicated phase, at pressure 99.2 kPa.[a]

w_{eqPS}[b]	Tg/K[c]	T_{et}/K[c]	T_l/K[c]	Phase field[d]
0.0462	192.3	260.6	272.4	Ice
0.1113	196.2	260.2	270.0	Ice
0.1554	196.5	258.8	268.2	Ice
0.2005		260.3	266.6	Ice
0.2500		257.5	267.3	$KHC_4H_4O_4$
0.2945	193.6	253.5	278.6	$KHC_4H_4O_4$
0.3000		253.3	282.5	$KHC_4H_4O_4$
0.3505		249.9	289.0	$KHC_4H_4O_4$
0.3959	193.8	245.7	297.7	$KHC_4H_4O_4$
0.4011	194.7	243.7	[e]	$KHC_4H_4O_4$
0.4496	195.3	239.6	[e]	$KHC_4H_4O_4$
0.4503		238.7	303.3	$KHC_4H_4O_4$
0.4503	194.4	233.9	[e]	$KHC_4H_4O_4$
0.4505		265.1	305.5	$KHC_4H_4O_4$
0.5008		237.9	[e]	$KHC_4H_4O_4$
0.5008	198.4	236.9	306.1	$KHC_4H_4O_4$

[a] Experimental pressure was not controlled beyond the typical range of atmospheric pressure, (99.2 ± 2.9) kPa (station pressure).
[b] Mass fraction uncertainty, U = 0.001 (0.95 confidence level).
[c] Temperature uncertainty, U = 2 K (0.94 confidence level).
[d] Melting of ice was identified by infrared (IR) spectroscopy of thin films as described in the Experimental Section. Identity of salt phase field is given by a combination of X-ray crystallography and IR analysis.
[e] The shape of the *liquidus* signal did not lead to a clear value for the *liquidus* transition.

present in all other samples we studied with transition temperatures corresponding to those identified in DSC experiments.

3.4. $K_2C_4H_4O_4/H_2O$

For this system, we studied solutions with target composition ranging from 0.05 to 0.5 *w* $K_2C_4H_4O_4$. In our DSC experiments, we observed crystallization occurred in both the cooling and warming segments for all samples. This was followed by a general pattern of eutectic and final melts in the warming segment. To determine the identity of the least soluble salt in our samples, we utilized X-ray crystallography. A single crystal from two samples of composition 0.4505 and 0.5008 *w* $K_2C_4H_4O_4$ were used for unit cell determination. In both cases the crystals were determined to be potassium hydrogen succinate by a match of the unit cell data in the CSD [23], which are listed in Table S1. This is an unexpected result for solutions that are 2:1 K^+:$C_4H_4O_4^{2-}$ where we would expect a compound of the same ratio to form. However, it is consistent with the other double potassium dicarboxylate systems we studied. Therefore, data for this system will be presented as "equivalent" mass fraction $K_2C_4H_4O_4$ and utilize the symbol w_{eqPS}. We considered the possibility that $HC_4H_4O_4^-$ may be a significant fraction of the ion composition in solution due its equilibria with the succinate ion in water. The pK_a of $HC_4H_4O_4^-$ is 5.61 resulting in a pK_b value for succinate ion of 8.39 [17]. Given the initial succinate ion concentrations in our solutions due to its stoichiometric neutralization with KOH, the succinate ion would be only 0.006–0.013% reacted to $HC_4H_4O_4^-$. Thus, presence of significant $HC_4H_4O_4^-$ is unlikely to be the explanation for $KHC_4H_4O_4$ crystals in our samples.

Raw DSC data are shown in Table 6. A typical thermogram for a solution in this system is given in Fig. S4 (w_{eqPS} = 0.3959). For nearly all samples, we observed warming crystallizations had substantial overlap with the eutectic melting, affecting its thermal signal and the calculated temperature of onset of the eutectic (tangent at half height of the eutectic endotherm extrapolated to the calculated baseline.) Additionally, for nearly all samples the shape of the eutectic melting endotherm (sloping thermal signal and significant difference between the "onset" and "peak" temperatures of the transition) indicated the sample had not completely crystallized. In some cases (higher composition samples) this may be partially due to the overlap of the warming crystallization that did not complete before melting began. In lower composition samples where the sample fell in the ice primary phase region, the warming crystallization had significant separation from the peak of the eutectic melt, thus overlap of the two transitions was unlikely the issue. In either case, the thermal evidence indicates that some liquid was always present in our samples along with ice and crystalized salt. Since the definition of a eutectic transition is onset of melting, the shape of the eutectic transitions in our thermograms necessarily led to lower calculated eutectic temperatures than would be expected. The *liquidus* and eutectic transitions determined from DSC experiments are shown in the constructed phase diagram of Fig. 6. It is seen that the "eutectic" transitions in the figure are much lower than those expected by an intersection of the *liquidus* curves, except for one. The *liquidus* data for each primary phase field were fit to Eq. (1) and the polynomial coefficients are given in Table 3. The two equations were solved simultaneously, and the eutectic point was calculated to be 0.2392 w_{eqPS} and 264.6 K. This is shown as a horizontal line in the phase diagram. For only one sample (0.4505 w_{eqPS}) the warming crystallizations did not overlap the eutectic melt, and it appears the entire sample froze before the eutectic transition. Thus, as seen in Fig. 6, the eutectic temperature determined from the thermogram (265.1 K) is in excellent agreement with the calculated value given above. We also observed glass transitions in many of our samples with an average onset value of (194.5 ± 1.6) K. In several cases the glass transition signal was too weak to determine quantitative temperature data.

Solubility in the analogous sodium salt system ($Na_2C_4H_4O_4$) has been reported by Linke [1], and we have included solubility data

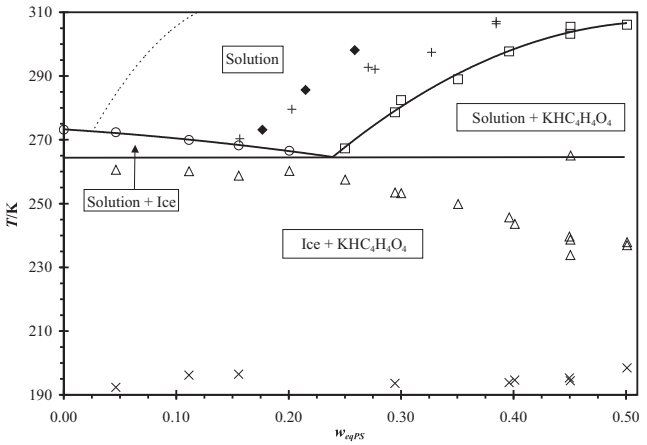

Fig. 6. Phase equilibria in aqueous solutions containing a 2:1 ratio of KOH:$H_2C_4H_4O_4$ constructed from our DSC and IR data; w_{eqPS} is the equivalent mass fraction $K_2C_4H_4O_4$. Symbols are: ○ ice melt; □ salt dissolution; △ calculated eutectic onset temperature from DSC analysis (see text), x onset glass transition temperature. Solid curves are fits to the data for the *liquidus* points; horizontal line is eutectic calculated from intersection of *liquidus* curves. Solids that form in this system are identified as ice and $KHC_4H_4O_4$ (see text). Plotted for comparison in units of mass fraction of the respective compound is solubility of the compound formed in 1:1 KOH:$H_2C_4H_4O_4$ solutions (+) from this study, and $Na_2C_4H_4O_4{\cdot}6H_2O$ (◆) solubility data from Linke [1]. Dotted line is a fit to the solubility of succinic acid also from Linke, and plotted as mass fraction of $H_2C_4H_4O_4$.

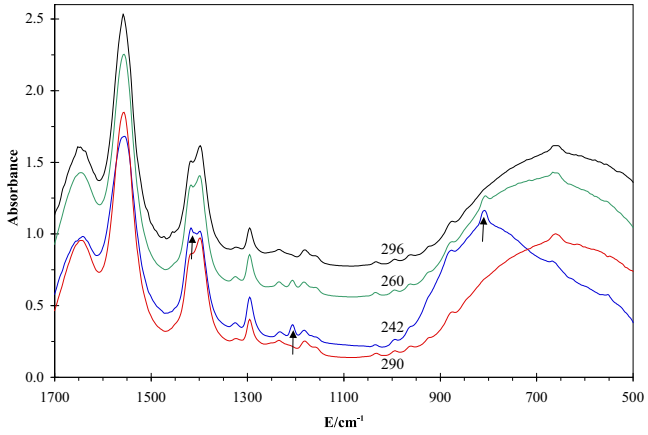

Fig. 7. Temperature series of infrared spectra for a 0.3959 w_{eqPS} sample where *E* represents energy. Temperature of each spectrum is given in the figure in Kelvin. For clarity, spectra are offset as follows: 290 K (0); 242 K (+0.1); 260 K (+0.45); 296 K (+0.65). Sample is initially all liquid at 290 K. Upon cooling it completely crystalized at 224 K with ice and $KHC_4H_4O_4$ forming (see text), after which warming was commenced. The bands we identified as characteristic of the salt and are indicated by arrows in the 242 K spectrum, which is during warming. The large OH absorption band at 855 cm^{-1} has moved back to the liquid position by 260 K. (see text for explanation of this transition). The salt continually dissolved upon further warming until characteristic absorption bands for the salt gradually shift to those observed in solution (296 K). We note it is difficult to determine the *liquidus* point for the salt in IR experiments as spectral changes become very subtle.

for this system as well as for succinic acid [1] in Fig. 6. The reported solid that forms in the $Na_2C_4H_4O_4/H_2O$ system at lower temperatures is $Na_2C_4H_4O_4{\cdot}6H_2O$, and it is seen in Fig. 6 this salt is less soluble than $KHC_4H_4O_4$. Both salts are more soluble than succinic acid. Thus, the presence of potassium ions in aqueous systems (where the pH is above 7 without sodium ions present) would allow succinate to remain in solution at much higher compositions than would be seen in acidic solutions or in the presence of sodium ions.

We utilized infrared spectroscopy to identify spectral features in our samples due to the formation of $KHC_4H_4O_4$. These experiments also allow us to identify the formation and melting of ice and thus corroborate transitions occurring in DSC experiments. A series of IR spectra taken at different temperatures is shown in Fig. 7 for the same sample used for the DSC experiment shown in Fig. S4 (0.3959 w_{eqPS}). Several spectral features appear to be characteristic of the salt as observed in many of our samples, and are indicated by arrows in the figure for a completely frozen sample: a shoulder at 1420 cm^{-1} grows and sharpens into a maximum creating a bifurcated band with maximum absorption at 1420 and 1399 cm^{-1}; a small band appears at 1208 cm^{-1} upon formation of the salt; a medium band appears at 807 cm^{-1} on top of the large, broad OH absorption band of ice. For samples in the salt primary phase region, these distinct bands appear upon crystallization of the salt and slowly fade as the salt dissolves into solution at the *liquidus* point when the sample is warmed. Thus, we take these absorption bands as characteristic of the presence of $KHC_4H_4O_4$ in this system, and we observed these features in our samples at other compositions.

We now note the differences in the characteristic data for $KHC_4H_4O_4$ formed in 2:1 KOH:$H_2C_4H_4O_4$ solutions and the solid(s) formed in 1:1 KOH:$H_2C_4H_4O_4$ solutions. As noted in Section 3.3, X-ray crystallographic unit cell data indicate two different crystals formed in a single solution: $KH_3(C_4H_4O_4)_2$ and $KHC_4H_4O_4$. A comparison of the eutectic temperature and concentration data for each system is given in Table S2 in the Supporting Information. It is seen the eutectic temperature is lower in the 2:1 system by 2.8 K, and the composition is higher by 0.0955 mass fraction (or 0.00936 mol fraction succinate ion). In addition, the most significant differences in the IR spectra for the solid formed in each system are listed in Table S3 and shown visually in Fig. S5 in the Supporting Information. Given these multiple differences and the evidence that $KHC_4H_4O_4$ forms in 2:1 KOH:$H_2C_4H_4O_4$ solutions, we conclude the compound forming from 1:1 KOH:$H_2C_4H_4O_4$ solutions is most likely not $KHC_4H_4O_4$, since the characteristic data do not match that for $KHC_4H_4O_4$ in 2:1 KOH:$H_2C_4H_4O_4$ solutions. Thus, we feel it is likely the predominant solid forming in 1:1 KOH:$H_2C_4H_4O_4$ solutions is $KH_3(C_4H_4O_4)_2$, and this conclusion is reflected in our analysis in Section 3.3.

3.5. $KHC_5H_6O_4/H_2O$

The samples we studied in this system ranged from 0.05 to 0.5 *w* $KHC_5H_6O_4$. Raw DSC data are provided in Table 7. In our DSC experiments, we observed some general trends when cooling and heating the samples. Melt/recrystallization events were observed below the eutectic in many samples indicating solids formed, thermally decomposed, and then the melt recrystallized. The average temperature of the melt/recrystallization event was (259.2 ± 0.2) K. The thermal signal for this sequence is shown in the thermogram given in Fig. S6 for a sample that is 0.3501 *w* $KHC_5H_6O_4$. In addition, many samples showed evidence of a second thermal decomposition of a solid at (264.6 ± 0.3) K. We strongly suspect this is a hydrate that thermally decomposes; however, we do not have clear evidence for the composition of this solid. These two transitions are then followed by what we identified as the eutectic melt and final melt of ice/salt dissolution by correlating the results of DSC and IR experiments (where the identity of solids can be determined). The average eutectic temperature from DSC experiments was determined to be 266.8 ± 0.3 K. The DSC data are plotted in Fig. 8 where a partial phase diagram is constructed. The *liquidus* points on both sides of the eutectic were fit to Eq. (1) and the resulting coefficients are given in Table 3. Solving these two equations simultaneously results in a eutectic composition of 0.3019 *w* $KHC_5H_6O_4$ and calculated temperature of 266.7 K, which is in excellent agreement with the experimental value.

Table 7
Phase transitions in the system $KHC_5H_6O_4/H_2O$ as determined by DSC experiments. Composition is given in mass fraction (w), T_{m1} is the onset of the first melt followed by a recrystallization, T_{m2} is an endothermic transition we identify as a thermal decomposition of an unstable solid, T_e is the eutectic temperature, and T_l is the *liquidus* temperature of the indicated phase, at pressure 99.2 kPa.[a]

w $KHC_5H_6O_4$[b]	T_{m1}/K[c]	T_{m2}/K[c]	T_e/K[c]	T_l/K[c]	Phase field[d]
0.0499		264.6	266.1	272.1	Ice
0.0975	258.6	264.3	266.2	271.1	Ice
0.1507		264.7	266.9	270.2	Ice
0.2002	259.3	264.1	267.0	268.7	Ice
0.2506		264.7	267.0	267.7	Ice
0.2737		264.6	267.0	267.0	Ice
0.2998	259.4	264.6	266.8	266.8	Ice
0.3115	259.0	264.1	266.7	271.0	$KHC_5H_6O_4$
0.3188		264.6	266.8	269.4	$KHC_5H_6O_4$
0.3260	259.3	264.6	267.1	[e]	$KHC_5H_6O_4$
0.3260	259.3	264.4	267.0	272.2	$KHC_5H_6O_4$
0.3344	259.3	264.4	266.8	273.5	$KHC_5H_6O_4$
0.3395	259.3	264.5	266.9	277.1	$KHC_5H_6O_4$
0.3501	259.4	264.6	266.8	279.6	$KHC_5H_6O_4$
0.3501	259.4	264.6	267.4	278.3	$KHC_5H_6O_4$
0.3720		264.6	266.7	283.9	$KHC_5H_6O_4$
0.3996	259.1	264.6	266.5	291.1	$KHC_5H_6O_4$
0.4202	259.3	264.7	266.7	296.5	$KHC_5H_6O_4$
0.4208		265.1	267.3	295.7	$KHC_5H_6O_4$
0.4488	256.63	264.6	266.5	[e]	$KHC_5H_6O_4$
0.4505		265.1	266.9	305.1	$KHC_5H_6O_4$
0.5000		264.6	266.5	[f]	$KHC_5H_6O_4$
0.5023		265.1	267.3	319.6	$KHC_5H_6O_4$

[a] Experimental pressure was not controlled beyond the typical range of atmospheric pressure, (99.2 ± 2.9) kPa (station pressure).
[b] Mass fraction uncertainty, U = 0.001 (0.95 confidence level).
[c] Temperature uncertainty, U = 2 K (0.94 confidence level).
[d] Melting of ice was identified by infrared (IR) spectroscopy of thin films as described in the Experimental Section. Identity of salt phase field is given by a combination of X-ray crystallography and IR analysis.
[e] The shape of the *liquidus* signal did not lead to a clear value for the *liquidus* transition.
[f] This sample was used for the X-ray crystallography analysis, but the DSC experiment was not run to a high enough temperature to determine the *liquidus* temperature.

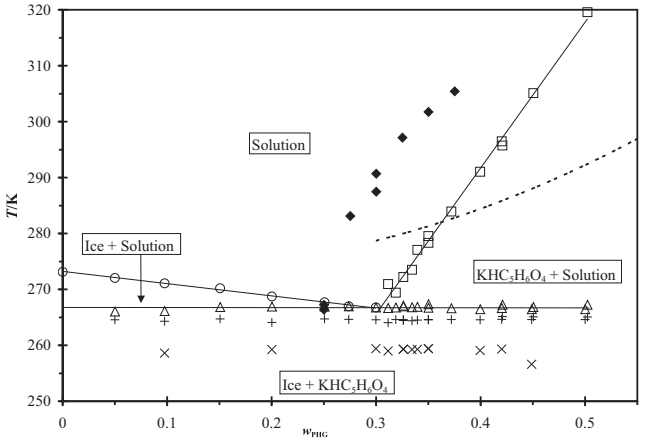

Fig. 8. Partial phase diagram for the $KHC_5H_6O_4/H_2O$ system constructed from our DSC data; w_{PHC} is the mass fraction of $KHC_5H_6O_4$. Symbols are: ○ ice melt, □ salt dissolution, △ eutectic transition, + solid thermal decomposition (see Section 3.5), x initiation of melt/recrystallization transition. Literature solubility data plotted as a function of the mass fraction of each species for comparison: ◆ $NaHC_5H_6O_4{\cdot}2H_2O$ [16], dotted line is a fit to the solubility data of $H_2C_5H_6O_4$ [25].

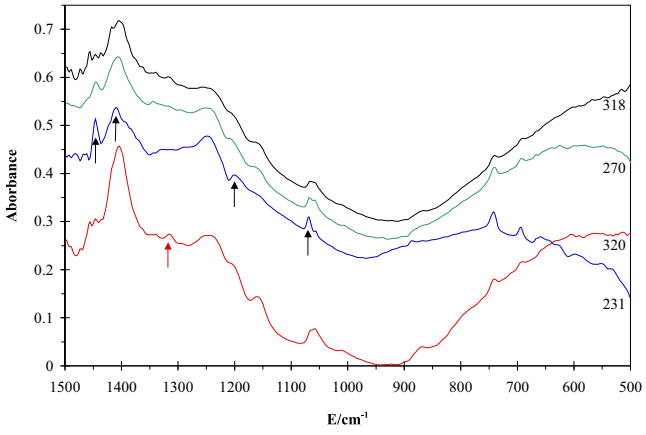

Fig. 9. Temperature series of infrared spectra for a 0.5000 w $KHC_5H_6O_4$ sample where E represents energy in wavenumbers (cm^{-1}). Temperature of each spectrum is given in the figure in Kelvin. For clarity, spectra are offset as follows: 320 K (−0.05); 231 K (+0.2); 270 K (+0.3); 318 K (+0.35). Sample is initially all liquid at 320 K. Upon cooling it completely crystalized at 231 K, after which warming was commenced. The bands we identified as characteristic of the salt and are indicated by arrows in the 231 K spectrum, which is during warming. Red arrow indicates a band that vanishes upon solution crystallization. The large OH absorption band at 855 cm^{-1} has moved back to the liquid position by 270 K. $KHC_5H_6O_4$ continually dissolved upon further warming until characteristic absorption bands for the salt gradually shift to those observed in solution at 318 K. (For interpretation of the references to colour in this figure legend, the reader is referred to the web version of this article.)

In order to identify the salt that formed in our samples we utilized X-ray crystallography; a single crystal that precipitated from a 0.5000 w $KHC_5H_6O_4$ solution was used for unit cell determination. The solid was determined to be $KHC_5H_6O_4$ by a match of the unit cell data [24] in the CSD, which are also listed in Table S1. We used the same solution before crystal formation for IR analysis. Spectra as a function of temperature for this sample are given in Fig. 9. We have noted the most significant shifts due to crystallization of $KHC_5H_6O_4$ with arrows in the figure. We observed these same shifts in our other samples, and thus used them to indicate formation of solid $KHC_3H_2O_4$, and their disappearance indicating dissolution of the solid. On the high energy side, we observed a very small band at 1447 cm^{-1} increases in intensity and

broadens slightly. The medium, broad band at 1405 cm^{-1} decreases and shifts to 1410 cm^{-1}. The band at 1314 cm^{-1} for the solution disappears when the sample freezes. The shoulder at 1205 cm^{-1} increases into a small, distinct absorption band. Lastly, the broad bifurcated band at (1066 and 1057) cm^{-1} shifts to a narrow peak and shoulder centered at 1070 and 1057 cm^{-1}, respectively. We observed other, smaller shifts as well, but these changes in the IR spectrum were the easiest to see. Thus, it was clear when eutectic and final melt (ice) or dissolution (salt) were observed in the IR spectra, which were then correlated with the transitions observed in the thermograms. We did not observe clear spectral evidence for the melt/recrystallization or pre-eutectic thermal decomposition transitions we observed in DSC experiments. It seems likely then, that the amount of substance undergoing these transitions is small compared to the fraction of the sample involved in the eutectic and *liquidus* transitions.

We previously studied solubilities in $NaHC_5H_6O_4/H_2O$ [16] and glutaric acid/H_2O [25] systems. The precipitating solid in the $NaHC_5H_6O_4/H_2O$ system was identified as $NaHC_5H_6O_4{\cdot}2H_2O$ and has a polymeric crystal structure. These data are shown on the phase diagram in Fig. 8 for comparison. It is seen that $NaHC_5H_6O_4{\cdot}H_2O$ is slightly less soluble than $KHC_5H_6O_4$. However, glutaric acid is more soluble than $KHC_5H_6O_4$ for T > 281 K. Thus, which compound glutarate ions precipitate as will depend on pH, temperature, and metal composition of the aqueous system.

3.6. $K_2C_5H_6O_4/H_2O$

This system was a challenge to study, and we again adopt the unit equivalent mass fraction (w_{eq}) for this system for reasons described below. The samples we studied ranged from 0.05 to 0.52 w_{eq} $K_2C_5H_6O_4$. Attempts at making higher composition samples failed as we were unable to get all component solids to dissolve even at elevated temperatures. We could not identify salt crystallization or dissolution in any of our IR experiments, indicating that any non-ice solids that formed were a very minor fraction of the crystalline phase. We observed two endothermic transitions for samples of 0.1 and 0.2 w_{eq} $K_2C_5H_6O_4$ in our DSC experiments. The thermogram for 0.2015 w_{eq} $K_2C_5H_6O_4$ is given in Fig. S7. It is clear from IR experiments the large endothermic transition is ice melting; thus, the additional endothermic transition at lower temperature may be a small amount of salt dissolving. However, we observed no characteristic absorption bands in IR experiments. Observing the shape of the thermogram (with a long sloping onset to the transition), it is clear there is liquid present in the sample throughout the warming segment; therefore, we conclude none of our samples completely froze. Thus, we have limited experimental results for this system and conclude there is a significant barrier to formation of any crystals in these solutions. Similar observations were reported by Beyer *et al.* [16] for the $Na_2C_5H_6O_4/H_2O$ system, where no crystallization of salt was observed.

3.7. Water activities

In a simple binary system, the freezing point depression can be used to determine solvent activities via the equation:

$$\ln a_w = -\int_{T_f}^{T_f^*} \frac{\Delta H_{fus}}{RT^2}\,dT \tag{3}$$

where a_w is the activity of water at T_f, ΔH_{fus} is the molar enthalpy of fusion of ice, R = 0.008314 kJ K^{-1} mol^{-1}, T_f is the depressed melting point, and T_f^* is the melting point of pure water. To a first approximation, the enthalpy of fusion can be considered constant as a function of temperature over few degrees; however, for larger temperature differences ΔH_{fus} needs to be expressed in terms of temperature so that the integral in Eq. (2) can be solved. Hobbs [26] lists values for ΔH_{fus} of ice at temperatures between 273 K and 251 K from the International Crititcal Tables [27]. We have fitted these data to a second order polynomial:

$$\Delta H_{fus} = \left(6.389 \times 10^{-4}\right)T^2 - -0.2534T + 27.56 \tag{4}$$

where T is in Kelvin and ΔH_{fus} is in kJ·mol^{-1}. This fit is quite good, reproducing the data in Hobbs to within 0.17% on average. Substituting Eqs. (3) into (2) and integrating yields:

$$\ln a_w = -\frac{1}{R}\left[6.389x10^{-4}\left(T_f^* - T_f\right) - 0.2534\ln\left(\frac{T_f^*}{T_f}\right) - 27.56\left(\frac{1}{T_f^*} - \frac{1}{T_f}\right)\right] \tag{5}$$

Finally, the activity coefficient (γ_w) can be calculated from the relationship:

$$\gamma_w = \frac{a_w}{x_w} \tag{6}$$

where x_w is the mole fraction of water. We followed this process for determining water activities and activity coefficients for systems we previously studied with good results [28]. We have determined water activities and activity coefficients in the systems studied here for samples where ice was the final melting phase using Eqs. (4) and (5) at T_f. The results are given in Fig. 10 where we have plotted mole fraction of water vs. water activity coefficient. Within experimental uncertainty, water in solutions of $KHC_3H_2O_4$ and $KHC_4H_4O_4$ (equivalent) acts ideally (γ_w = 1) in the ice primary phase field in each system. Water in solutions of $KHC_5H_6O_4$ deviates modestly from ideal for x_w < 0.98. The most significant deviations from ideal are seen in solutions that were 2:1 KOH: organic acid. It is seen in the figure that water activity coefficients are similar in these solutions (labeled $K_2C_3H_2O_4$ (equivalent), $K_2C_4H_4O_4$ (equivalent), and $K_2C_5H_6O_4$ (equivalent) in the figure caption), with $K_2C_3H_2O_4$ solutions deviating less from ideal than $K_2C_5H_6O_4$ or $K_2C_4H_4O_4$ solutions. The $K_2C_3H_2O_4$ solutions cover a wider concentration range than the other systems we studied (since no salt was observed to form, only ice), and deviations from ideal were less than the succinate or gultarate systems over the same x_w range. Within experimental uncertainty no values of γ_w were found to be greater than unity.

We previously reported the water activity coefficients for aqueous solutions of dicarboxylic acids. We observe that over the same

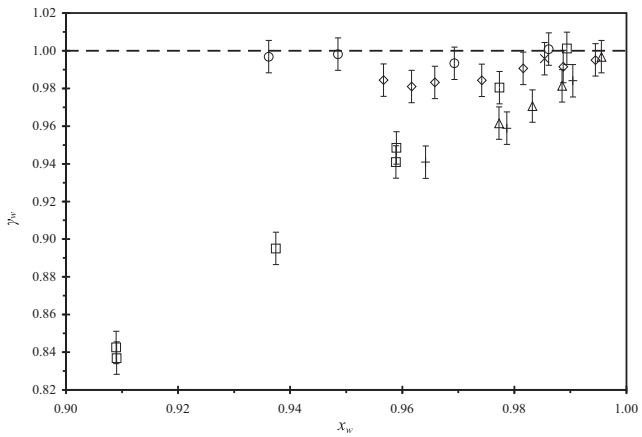

Fig. 10. Plot of water mole fraction (x_w) vs. water activity coefficient (γ_w) as calculated using Eqs. (4) and (5) in the text for systems studied in this paper. Symbols are for aqueous systems: ○ $KHC_3H_2O_4$, □ $K_2C_3H_2O_4$ (equivalent), x $KHC_4H_4O_4$ (equivalent), △ $K_2C_4H_4O_4$ (equivalent), ◇ $KHC_5H_6O_4$, + $K_2C_5H_6O_4$ (equivalent). Activity coefficient uncertainties are given by vertical error bars.

water mole fraction shown in Fig. 10, malonic acid did not show significant deviation from ideal behaviour [20]. Since succinic acid is weakly soluble in water, water activity data covers a much narrower composition range, and γ_w was found to be unity at $x_w > 0.986$ [25]. Glutaric acid presents a more complicated picture and γ_w values in the ice primary phase field have been determined to be greater than unity with values derived from several different types of experiments and theoretical predictions [25]. Over the range of water mole fraction shown in Fig. 10, the activity coefficient ranged from γ_w = 1.002 at x_w = 0.991 to γ_w = 1.032 at x_w = 0.904. This is in significant contrast to the water activities in our solutions involving glutarate ions, where $\gamma_w < 1$ for both 1:1 and 2:1 KOH:$H_2C_5H_6O_4$ solutions. In malonate, succinate, and glutarate systems studied here, it appears evident that the presence of potassium ions has a strong effect on water activity in these solutions, with larger fractions of potassium ions correlating with larger deviations from ideal.

4. Conclusions

We have studied the individual phase equilibria in aqueous solutions of 1:1 and 2:1 KOH and dicarboxylic acids: malonic, succinic, and glutaric. While we found the single potassium salts readily formed in the systems we studied here (where ratios of K^+/organic anion were both 1 and 2), we had no evidence for the formation of the double salts. Rather, no salt formation was observed in 2:1 K^+:$C_3H_2O_4^{2-}$ or K^+:$C_5H_6O_4^{2-}$ aqueous solutions. In the case of 2:1 aqueous solutions of K^+:$C_4H_4O_4^{2-}$, XRD unit cell data indicated the salt formed was $KHC_4H_4O_4$. In 1:1 KOH:$H_2C_4H_4O_4$ two crystals were identified: $KH_3(C_4H_4O_4)_2$ and $KHC_4H_4O_4$. Experimental evidence led us to conclude the majority compound formed is $KH_3(C_4H_4O_4)_2$, but further work on this system and the coexistence of these two compounds in aqueous solution is recommended.

In general, we found the potassium salts to be at least as soluble ($KH_3(C_4H_4O_4)_2$), or more soluble ($KHC_4H_4O_4$, $KHC_3H_2O_4$, $KHC_5H_6O_4$) than their analogous sodium salts. The potassium salts were also more soluble than their parent acids except in some cases where they were more soluble only at low temperatures ($KHC_3H_2O_4$, $KHC_5H_6O_4$), and so exhibit a temperature where the solubilities are equal, and above which the acid is more soluble. In two systems, we were unable to determine salt solubilities as salt formation was not observed (2:1 KOH:$H_2C_3H_2O_4$), or no salt formation was observed in the salt primary phase region (2:1 KOH:$H_2C_5H_6O_4$). These observations indicate the difficulty of forming double potassium salts in aqueous solution. In addition, water in the 2:1 KOH:organic acid solutions acts much less ideal than in the 1:1 solutions. This has significant implications for water vapor pressure over these solutions, indicating increasing potassium ion content will decrease the water vapor pressure, most significantly in solutions containing succinate ion and glutarate ions.

We also report IR spectra with characteristic absorption bands for each salt in systems where they formed. These absorption bands can be used to identify the presence of the various solids we observed in our experiments and confirmed via crystallographic unit cell parameter matching.

Funding: This work was supported by the National Science Foundation (USA) Atmospheric Chemistry Program (AGS-1361592)

Declaration of Competing Interest

The authors declare that they have no known competing financial interests or personal relationships that could have appeared to influence the work reported in this paper.

Acknowledgement

We wish to thank Dr. Anastasiya Vinokur and Dr. Ilia A. Guzei at the University of Wisconsin-Madison for performing the X-ray crystallography experiments.

Appendix A. Supplementary data

Supplementary data to this article can be found online at https://doi.org/10.1016/j.jct.2021.106466.

References

[1] W.F. Linke, Solubilities: inorganic and metal organic compounds: A revision and continuation of the compilation by A. Seidell. Fourth Edition. TWO VOLUMES, 4th edition, Van Nostrand, 1958.
[2] H. Stephen, T. Stephen, Solubilities of inorganic and organic compounds, Pergamon Press, Macmillan, [Oxford] New York, 1963.
[3] H. Silcock, Solubilities of Inorganic and Organic Compounds, Pergamon Press, Oxford, 1979.
[4] Clarivate Analytics, www.webofknowledge.com, (n.d.). www.webofknowledge.com.
[5] D.M. Murphy, D.S. Thomson, T.M.J. Mahoney, In Situ measurements of organics, meteoritic material, mercury, and other elements in aerosols at 5 to 19 Kilometers, Science. 282 (1998) 1664–1669.
[6] K.D. Froyd, D.M. Murphy, P. Lawson, D. Baumgardner, R.L. Herman, Aerosols that form subvisible cirrus at the tropical tropopause, Atmos. Chem. Phys. 10 (2010) 209–218, https://doi.org/10.5194/acp-10-209-2010.
[7] R.C. Sullivan, K.A. Prather, Investigations of the diurnal cycle and mixing state of oxalic acid in individual particles in asian aerosol outflow, Environ. Sci. Technol. 41 (2007) 8062–8069, https://doi.org/10.1021/es071134g.
[8] T. Kojima, P.R. Buseck, Y. Iwasaka, A. Matsuki, D. Trochkine, Sulfate-coated dust particles in the free troposphere over Japan, Atmospheric Res. 82 (2006) 698–708, https://doi.org/10.1016/j.atmosres.2006.02.024.
[9] J.S. Reid, R. Koppmann, T.F. Eck, D.P. Eleuterio, A review of biomass burning emissions part II: Intensive physical properties of biomass burning particles, Atmos. Chem. Phys. 5 (2005) 799–825, https://doi.org/10.5194/acp-5-799-2005.
[10] M.D. Zauscher Y. Wang M.J.K. Moore C.J. Gaston K.A. Prather A.Q. Impact P. Aging of Biomass Burning Aerosols during the, San Diego Wildfires Environ. Sci. Technol. 47 2013 2007 7633 7643 10.1021/es4004137
[11] V.-M. Kerminen, K. Teinilä, R. Hillamo, T. Pakkanen, Substitution of chloride in sea-salt particles by inorganic and organic anions, J. Aerosol Sci. 29 (1998) 929–942, https://doi.org/10.1016/S0021-8502(98)00002-0.
[12] A. Laskin, R.C. Moffet, M.K. Gilles, J.D. Fast, R.A. Zaveri, B. Wang, P. Nigge, J. Shutthanandan, Tropospheric chemistry of internally mixed sea salt and organic particles: Surprising reactivity of NaCl with weak organic acids, J. Geophys. Res. 117 (2012) D15302, https://doi.org/10.1029/2012JD017743.
[13] S. Ghorai, B. Wang, A. Tivanski, A. Laskin, Hygroscopic properties of internally mixed particles composed of NaCl and water-soluble organic acids, Environ. Sci. Technol. 48 (2014) 2234–2241, https://doi.org/10.1021/es404727u.
[14] B. Wang, R.E. O'Brien, S.T. Kelly, J.E. Shilling, R.C. Moffet, M.K. Gilles, A. Laskin, Reactivity of liquid and semisolid secondary organic carbon with chloride and nitrate in atmospheric aerosols, J. Phys. Chem. A. 119 (2015) 4498–4508, https://doi.org/10.1021/jp510336q.
[15] J.A. Kissinger, L.G. Buttke, A.I. Vinokur, I.A. Guzei, K.D. Beyer, Solubilities and glass formation in aqueous solutions of the sodium salts of malonic acid with and without ammonium sulfate, J. Phys. Chem. A. 120 (2016) 3827–3834, https://doi.org/10.1021/acs.jpca.6b02656.
[16] K.D. Beyer, L.G. Buttke, Solubilities in aqueous solutions of the sodium salts of succinic and glutaric acid with and without ammonium sulfate, J. Chem. Thermodyn. 125 (2018) 189–199, https://doi.org/10.1016/j.jct.2018.06.002.
[17] D.R. Lide, Handbook of Chemistry and Physics, CRC Press, Boca Ratan, 1993.
[18] M. Schubnell, Temperature and heat flow calibration of a DSC-instrument in the temperature range between-100 and 160 Degrees C, J. Therm. Anal. Calorim. 61 (2000) 91–98.
[19] M. Currie, J.C. Speakman, The crystal structures of the acid salts of some dibasic acids. Part III. Potassium hydrogen malonate: a neutron diffraction study, J. Chem. Soc. Inorg. Phys. Theor. (1970) 1923–1926, https://doi.org/10.1039/J19700001923.
[20] A.R. Hansen, K.D. Beyer, Experimentally determined thermochemical properties of the malonic acid/water system: Implications for atmospheric aerosols, J. Phys. Chem. A. 108 (2004) 3457–3466.
[21] I.A. Guzei, Potassium Malonate Crystal, Structure (2020).
[22] R.S. Dunlop, J.C. Speakman, The crystal structure of, and the hydrogen bonding in, the super-acid salt potassium tri-hydrogen di-succinate: a direct solution of the phase problem based on neutron-diffraction measurements*, Z. Für Krist. - Cryst. Mater. 138 (1973) 100–112, https://doi.org/10.1524/zkri.1973.138.1-4.100.
[23] A. McAdam, M. Currie, J.C. Speakman, The crystal structures of the acid salts of some dibasic acids. Part IV. Potassium hydrogen succinate: X-ray and neutron-

diffraction studies, J. Chem. Soc. Inorg. Phys. Theor. (1971) 1994–1997, https://doi.org/10.1039/J19710001994.
[24] A.L. Macdonald, J.C. Speakman, Rubidium hydrogen glutarate and ammonium hydrogen glutarate: X-ray studies of quasi-isostructural crystals involving very short hydrogen bonds, J. Cryst. Mol. Struct. 1 (1971) 189–198, https://doi.org/10.1007/BF01198531.
[25] K.D. Beyer, K. Friesen, J.R. Bothe, B. Palet, Phase Diagrams and Water Activities of Aqueous Dicarboxylic Acid Systems of Atmospheric Importance, J. Phys. Chem. A. 112 (2008) 11704–11713.
[26] P.V. Hobbs, Ice Physics, Oxford University Press, London, 1974.
[27] National Research Council (U.S.), E.W. Washburn, C.J. West, C. Hull, International council of scientific unions. [from old catalog], National academy of sciences Washington D.C. [from old catalog], International critical tables of numerical data, physics, chemistry and technology, Pub. for the National research council by the McGraw-Hill book company, inc, New York [etc.], 1926.
[28] K.D. Beyer, M. Richardson, B. Reusch, Phase diagrams and water activities of aqueous ammonium salts of malonic acid, J. Phys. Chem. A. 115 (2011) 3042–3049, https://doi.org/10.1021/jp200191t.

JCT D-20-00103